Supporting Information

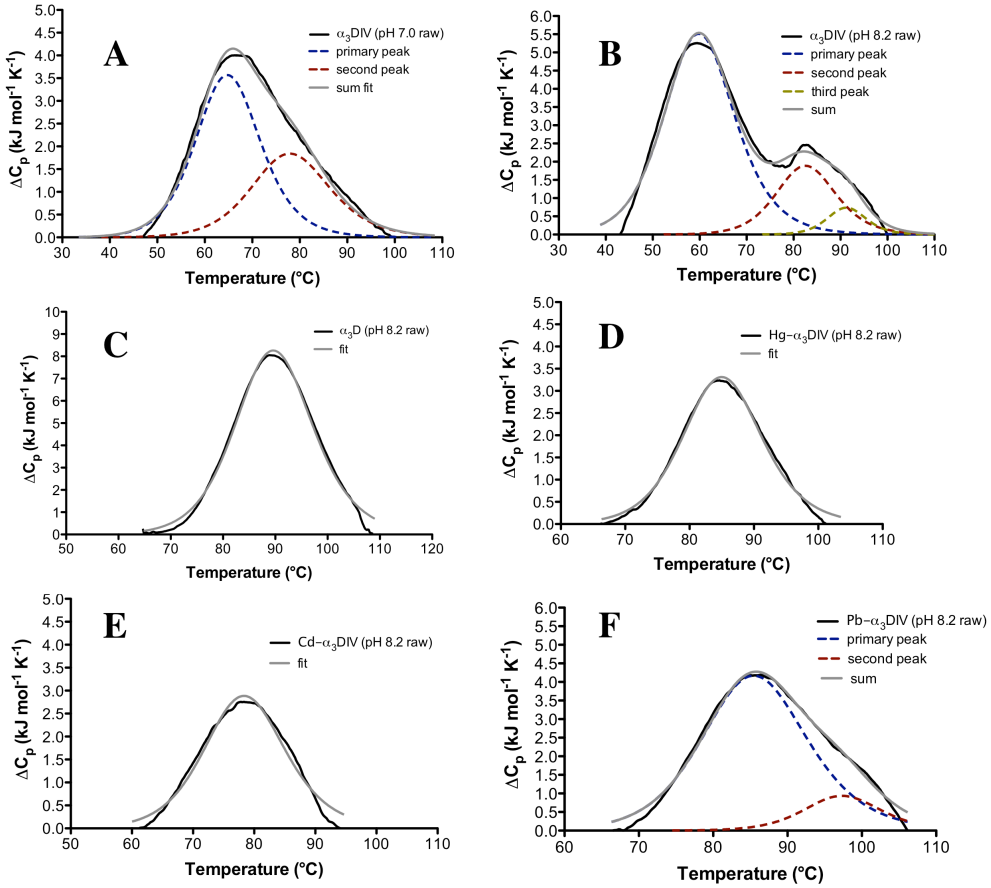

SI FIGURE 1: (A) Thermal denaturation curve of apo α_3D**IV** at pH 7.0 fitted to a two-peak model. (B) Thermal denaturation curve of apo α_3D**IV** at pH 8.2 fitted to a three-peak model. (C) Thermal denaturation curve of α_3D at pH 8.2 fitted to a one-peak model. (D) Thermal denaturation curve of Hg-α_3D**IV** at pH 8.2 fitted to a one-peak model. (E) Thermal denaturation curve of Cd-α_3D**IV** at pH 8.2 fitted to a one-peak model. (F) Thermal denaturation curve of Pb-α_3D**IV**at pH 8.2 fitted to a two-peak model.

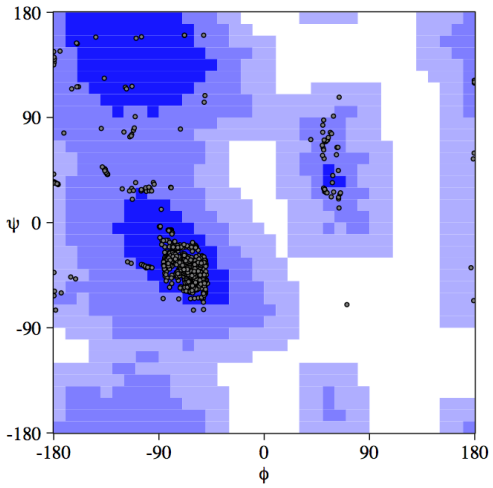

SI FIGURE 2: Procheck-NMR Ramachandran plot of the 20 lowest structures exhibits that 90.1% of the backbone stereochemistry is located in the most favored, 7.8% in additionally allowed regions, 2.0% in generously allowed and 0.1% in disallowed regions.

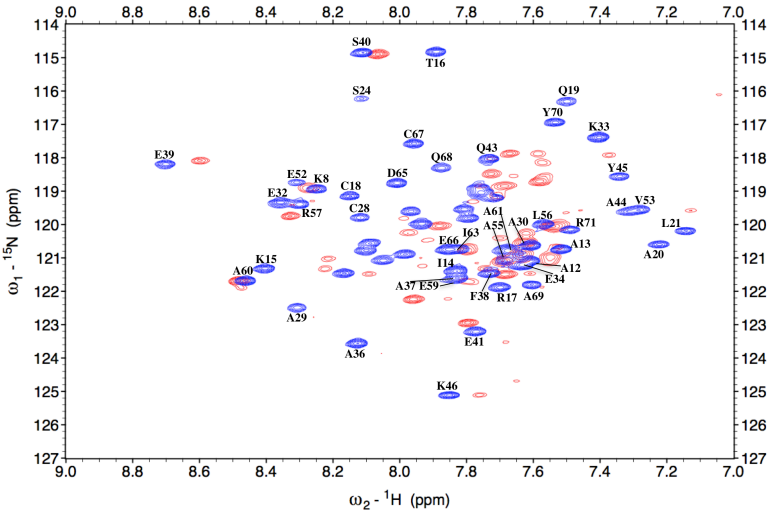

SI FIGURE 3: Enlargement of the ^{15}N-HSQC spectra of apo α_3D**IV** (blue) and Hg(II)-α_3D**IV** (red), both at pH 8.6. Spectra were collected on a 500 MHz Varian VNMRS NMR system at 9 °C. The peaks that were assigned in the apo spectrum are labeled. At this high pH condition, a reduction in the chemical shift peaks for both spectra were

expected as the backbone proton kinetic exchange rate increases with pH. Thereby, these experiments were collected at 9 °C in order to decrease the exchange rate and regain missing resonance peaks. In this view, the apo spectrum displayed 54 peaks of 55 that were identified, whereas the Hg-α_3D**IV** spectrum contained 47 peaks.

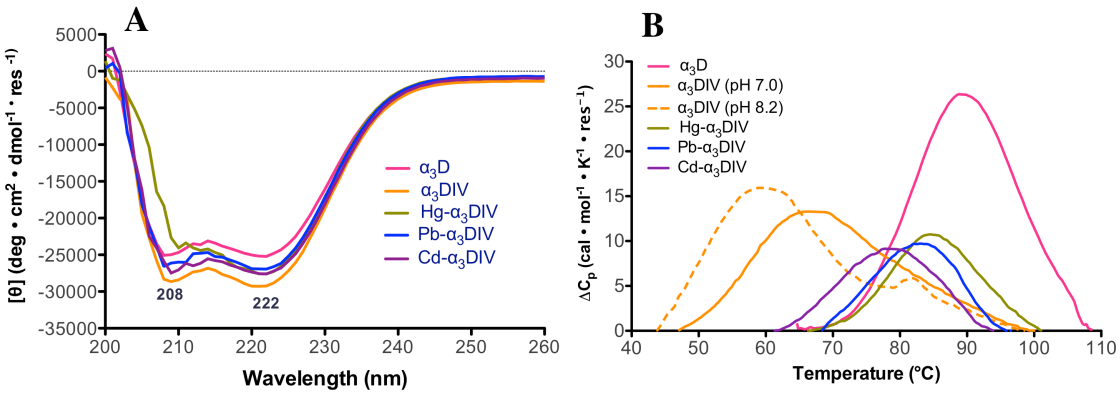

SI FIGURE 4: (A) CD spectrum of α_3D (pink), α_3D**IV** (orange), Hg(II)-α_3D**IV** (green), Pb(II)-α_3D**IV** (blue) and Cd(II)-α_3D**IV** (purple). Each spectrum contains a double minima at 208 and 222 nm and [θ] molar ellipticity values typical for a well-folded α-helical structure. (B) Thermograms of α_3D (pink), α_3D**IV** at pH 7.0 (orange), α_3D**IV** at pH 8.2 (dashed orange), Hg(II)-α_3D**IV** (green), Pb(II)-α_3D**IV** (blue), and Cd(II)-α_3D**IV** (purple). The metallated species had melting temperatures ~20 °C higher than the apo.

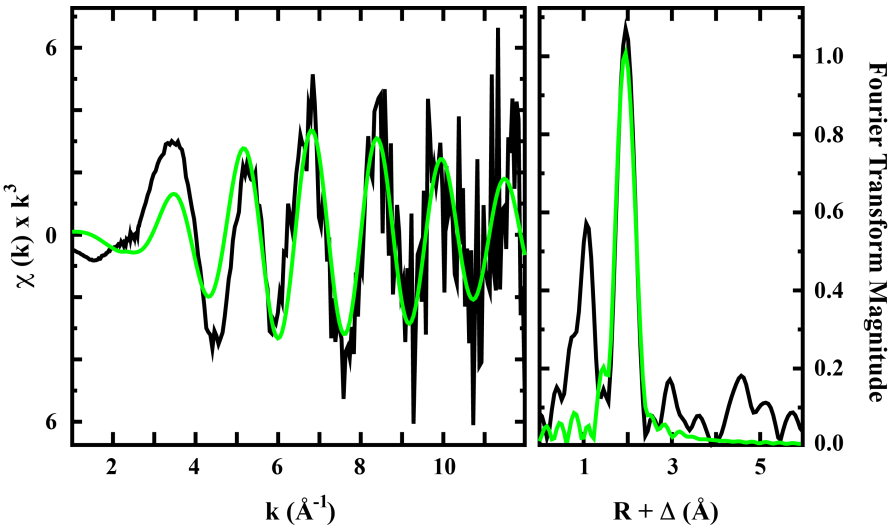

SI FIGURE 5: EXAFS and Fourier Transform for Hg-α_3D**IV**. (Left) Raw unfiltered EXAFS data (black) and simulations (green) for Hg-α_3DIV. (Right) Fourier transforms of the raw EXAFS (black) and best fit simulation (green) for Hg-α_3DIV.

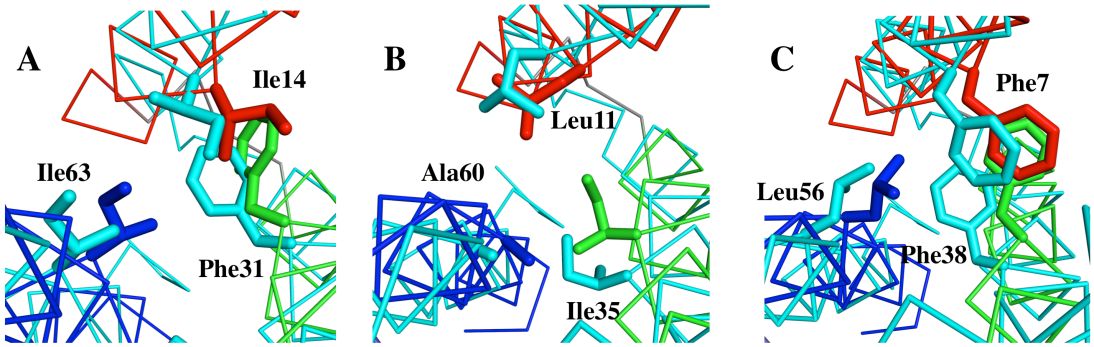

SI FIGURE 6: (A) First layer of apolar groups (α_3D**IV** red: helix1, green: helix2, and blue: helix3; α_3D: cyan) above positions 18, 28, and 67, which involves Ile14, Phe31, and Ile63. (B) Second layer of apolar groups, Leu11, Ile35, and Ala60. (C) Third layer of apolar groups, Phe7, Phe38, and Leu56.

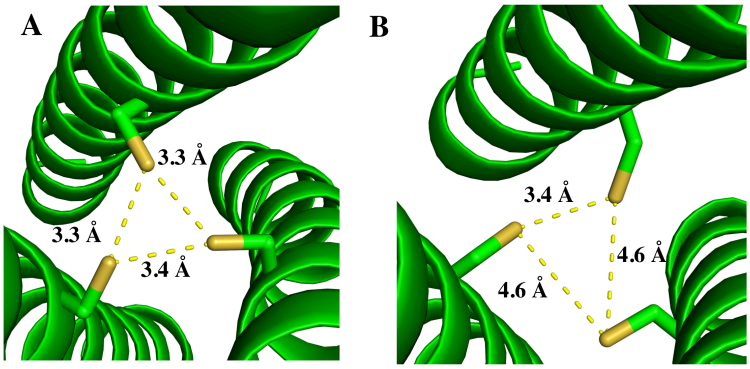

SI FIGURE 7: (A) "a" site Cys in apo CSL9C[60] (PDB 3LJM), in which the Sγ atoms position inside the core. The alternate conformation of the Sγ atoms was removed in order to illustrate the orientation of "a" site Cys residues. (B) "d" site Cys in apo CSL19C[60] (PDB 2X6P), which contain Sγ atoms that point at the interhelical interface.

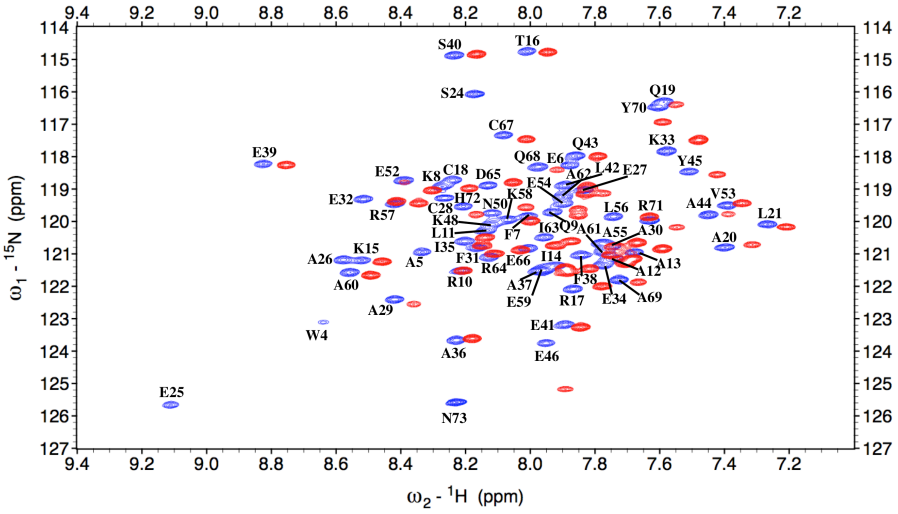

SI FIGURE 8: Enlargements of ^{15}N-HSQC spectra of apo α_3D**IV** pH 5.8 (blue) and pH 8.6 (red). Spectra were collected on a 500 MHz Varian VNMRS NMR instrument at 25 °C. The pH 5.8 spectrum contains 64 of the 68 total peaks and the assignments are adjacent to its peak, whereas the pH 8.6 spectrum has 54 of the 55 identified peaks (not

assigned). The peaks at pH 8.6 shift upfield of pH 5.8 and also contain 15 less identifiable peaks, demonstrating a pH effect on the hydrogen exchange rates.

SI Table 1: Acquisition Parameters for NMR Experiments Performed on α_3D**IV**.

	no. of acquired data points (nucleus)			spectral width (Hz)				
experiment	t_1	t_2	t_3	F_1	F_2	F_3	nt	Ref[b]
2D ^{1}H–^{15}N TROSY	400 (^{15}N)	4102 (^{1}H)		3000	12019		2	27-29
3D HNCO TROSY	150 (^{13}C)	40 (^{15}N)	2396 (^{1}H)	2750	2500	12019	2	30
3D HN(CA)CO	150 (^{13}C)	80 (^{15}N)	2368 (^{1}H)	2750	2500	12019	4	30
3D HNCA	150 (^{13}C)	80 (^{15}N)	2396 (^{1}H)	5500	2500	12019	4	31
3D HN(CO)CA	150 (^{13}C)	80 (^{15}N)	2396 (^{1}H)	5500	2500	12019	2	31
3D HNCACB	300 (^{13}C)	80 (^{15}N)	2396 (^{1}H)	15001	2500	12019	8	32, 33
3D HN(CO)CACB	300 (^{13}C)	80 (^{15}N)	2396 (^{1}H)	15001	2500	12019	8	32, 33
3D HN(CA)HA[a]	200 (^{1}H)	60 (^{15}N)	4102 (^{1}H)	2500	2500	12019	4	34
3D HC(C)H–COSY[a]	128 (^{1}H)	200 (^{13}C)	2048 (^{1}H)	5500	16000	15060	4	36
3D HC(C)H–TOCSY	200 (^{13}C)	100 (^{13}C)	2048 (^{1}H)	16000	16000	15060	4	37, 38
3D ^{15}N NOESY TROSY	200 (^{1}H)	80 (^{15}N)	4102 (^{1}H)	8000	2500	12019	8	39
3D HMQC NOESY TROSY	200 (^{13}C)	80 (^{15}N)	4102 (^{1}H)	14000	2500	12019	12	40
3D ^{15}N NOESY TROSY[a]	200 (^{1}H)	100 (^{13}C)	2048 (^{1}H)	9000	16000	15060	4	39
3D NOESY ^{13}CHSQC[a]	150 (^{1}H)	200 (^{13}C)	2048 (^{1}H)	7500	16000	15060	4	39
3D NOESY ^{13}C TROSY	72 (^{13}C)	80 (^{15}N)	4102 (^{1}H)	7000	2500	12019	4	39
3D NOESY (^{13}C) TROSY	72 (^{1}H)	80 (^{15}N)	4102 (^{1}H)	2000	2500	12019	4	39

[a]In-phase and anti-phase experiment. [b]References from the main document.

SI Table 2: Summary of Hg EXAFS fitting analysis for Hg-α_3D**IV**.

	Nearest Neighbor Ligand Environment[a]				
Complex	**Atom**[b]	**R (Å)**[b]	**C. N.**[d]	**σ^2**[e]	**F**[f]
Hg-α_3D**IV**	S	2.36	2.0	3.54	2.24
	S	**2.36**	**2.5**	**4.97**	2.21
	S	2.36	3.0	6.20	2.21

Data fit over a k range of 1 to 12 Å-1. Best fit simulation parameters are in bold. [a]Independent metal-ligand scattering environment at R < 3.0 Å. [b]Scattering atoms: S (Sulfur). [c]Average metal-ligand bond length for 2 independent samples. [d]Average metal-ligand coordination number for 2 independent samples. [e]Average Debye-Waller factor in Å^2 x 10^3 for 2 independent samples. [f]Number of degrees of freedom weighted mean square deviation between data and fit.

SI Table 3. Ramachandran Plot Summary for residues 1-73 from PSVS analysis.

	Procheck		Richardson Lab's Molprobity	
	α_3D**IV**	α_3D	α_3D**IV**	α_3D
Most favored regions	89.2%	86.2%	93%	81.7%
Allowed regions	9.2%	10.8%	4.2%	15.5%
Generously allowed regions	1.5%	1.5%		
Disallowed regions	0.0%	1.5%	2.8%	2.8%

SI Table 4. PSVS global quality scores for 20 structures of α_3D**IV**, structure 1 of α_3D**IV** and structure 1 of α_3D.

			20 structures α_3D**IV**		
Program	**Verify3D**	**ProsaII (-ve)**	**Procheck (phi-psi)**[a]	**Procheck (all)**[a]	**Molprobity Clashscore**
Raw Score	0.47	1.35	0.09	-0.40	15.39
Z-Score[b]	0.16	2.89	0.67	-2.37	-1.12
			Structure 1 α_3D**IV**		
Raw Score	0.47	1.45	0.02	-0.37	17.95
Z-Score[b]	0.16	3.31	0.39	-2.19	-1.55

Close Contacts and Deviations from Ideal Geometry (PDB validation software)

Number of close contacts (within 1.6 Å for H atoms & 2.2 Å for heavy atoms	0
RMS deviation for bond angles	0.2°
RMS deviation for bond lengths	0.001 Å

			Structure 1 α_3D		
Raw Score	0.55	1.29	-0.64	-0.98	68.48
Z-Score[b]	1.44	2.65	-2.20	-5.80	-10.23

Close Contacts and Deviations from Ideal Geometry (PDB validation software)

Number of close contacts (within 1.6 Å for H atoms & 2.2 Å for heavy atoms	0
RMS deviation for bond angles	2.6°
RMS deviation for bond lengths	0.020 Å

[a]For all residues. [b]With respect to mean and standard deviation for a set of 252 X-ray structures <500 residues of resolution of 1.80 Å, R-factor of 0.25 and R-free of 0.28; a positive value indicates a "better" score."

SI Table 4: Thermal denaturation parameters.

Protein	α_3D[a]	α_3D**IV**[b]	α_3D**IV**[a]	Hg-α_3D**IV**[a]	Pb-α_3D**IV**[a]	Cd-α_3D**IV**[a]
T_m (°C)	89.6 (0.3)	**64.4 (0.6)** 76.1 (1.9)	**60.2 (0.1)** 82.2 (0.8) 89.9 (2.1)	84.0 (1.7)	**83.4 (3.3)** 92.0 (7.7)	78.1 (0.7)
ΔH_{calc} (kcal mol^{-1})	49.9 (4.6)	**50.0 (0.2)** 46.1 (1.4)	**44.9 (1.2)** 60.0 (0.5)	65.1 (3.5)	**59.2 (6.9)** 104.2 (35.1)	52.7 (4.3)
$\Delta H_{van't\ Hoff}$ (kcal mol^{-1})	41.2 (4.8)	**20.8 (3.1)** 15.8 (2.7)	**23.5 (2.1)** 8.5 (2.1) -	10.3 (3.1)	**14.6 (6.0)** 5.9 (1.5)	12.6 (0.6)

All the averaged values were determined from triplicate or duplicate experiments. Bolded values indicate primary denaturation species. [a]pH 8.2. [b]pH 7.0.

SI Table 5 Metrical parameters of Hg-S bonds in model compounds.

Compound	**Hg-S R (Å)**	**Hg-S R (Å)**	**Hg-S R (Å)**	**ref**
Trigonal T-shaped HgS_3				
catena-(bis(O-methyldithiocarbonato-S)-mercury(ii))	2.365	2.383	2.924	1
tetra-n-butylammonium (3-ethoxycarbonylthiolato-4,5-diphenylthiophene-2-thiolato)-(4,5-diphenylthiophene-2,3-dithiolato)-mercury(ii)	2.373	2.388	2.495	2
(thiocyanato)-bis(4-trimethylammoniobenzenethiolato) -mercury(ii) hexafluorophosphate	2.353	2.369	2.823	3
Average 3 M-L		2.497 (0.071)		
Trigonal HgS_3				
tetra-n-butylammonium tris(phenylthiolato-S)-mercury(ii)	2.407	2.432	2.507	4
catena-(ethylenediammonium tris(m2-sulfido)-sulfido-mercury-tin)	2.396	2.435	2.653	5
Tetraethylammonium tris(t-butylthiolato-S)-mercury(ii)	2.436	2.438	2.451	6

tetrakis(n-Propylammonium) tris((2,4,6-tri-isopropyl)benzenethiolato)-mercury methanol solvate	2.398	2.46	2.47	7
Tetraphenylphosphonium tris(2,3,5,6-tetramethylbenzenethiolato-S)-mercury acetonitrile solvate	2.397	2.404	2.493	8
Tetramethylammonium bis(tris(m2-thiobenzoato-O,S)-mercury(ii))-sodium	2.443	2.468	2.485	9
bis(Tetraethylammonium) (m2-benzene-1,2-dithiolato-S,S')-bis(benzene-1,2-dithiolato)-di-mercury(ii)	2.382	2.429	2.437	10
Tetraethylammonium tris(cyclohexylthiolato-S)-mercury	2.403	2.455	2.487	11
Average 3 M-L		2.449 (0.023)		
HgS_2 model references				
bis(carboxymethylthiolato)-mercury(ii)	2.339	2.339		12
bis(n-Pentanethiolato)-mercury(ii)	2.304	2.304		13
catena-(bis(m2-Bromo)-bis(m2-N,N-diethyldithiocarbamato-S,S')-di-mercury)	2.364	2.385		14
bis(2-Mercaptobenzoato-S)-mercury(ii) dioxane solvate	2.363	2.363		15
bis(4-t-Butylbenzenethiolato-S)-mercury(ii)	2.358	2.363		16
Average 2 M-L		2.348 (0.028)		

The Hg(II)-S bond lengths represent one complex within a network.

1. Tiekink, E. R. T. (1987) Bis(O-methyldithiocarbonato)mercury(II). *Acta Crystallogr., Sect. C: Cryst. Struct. Commun. 43*, 448 – 450.

2. Kim, Y.-Y., Lee, H.-H., Nam, H.-J, and Noh, D.-Y. (2001) Mononuclear three-coordinate mercury(II)-thiolate complex: synthesis and X-ray crystal structure. *Bull. Korean Chem. Soc. 22*, 17 – 18.

3. Chen, J.-X., Zhang, W.-H., Tang, X.-Y., Ren, Z-G., Zhang, Y., and Lang, J. P. (2006) Assembly of a New Family of Mercury(II) Zwitterionic Thiolate Complexes from a

Preformed Compound $[Hg(Tab)_2](PF_6)_2$ [Tab) 4-(Trimethylammonio)benzenethiolate]. *Inorg. Chem. 45*, 2568 – 2580.

4. Christou, G., Folting, K., and Huffman, J. C. (1984) Mononuclear, three-coordinate metal thiolates: Preparation and crystal structures of $[NBu^n_4][Hg(SPh)_3]$ and $[NPr^n_4][Pb(SPh)_3]$. *Polyhedron 3*, 1247 – 1253.

5. Wang, Y.-Y., Baiyin, M.-H., Ji, S.-H., Liu, X.-Y., An, Y-.L., and Ning, G.-L. (2006) Solvothermal Synthesis and Characterization of $(NH_3CH_2CH_2NH_3)HgSnS_4$ with a Column Structure. *Chem. Res. Chin. Univ. 22*, 411 – 414.

6. Watton, S. P., Wright, J. G., MacDonnell, F. M., Bryson, J. W., Sabat, M. and O'Halloran, T. V. (1990) Trigonal mercuric complex of an aliphatic thiolate: a spectroscopic and structural model for the receptor site in the mercury(II) biosensor MerR. *J. Am. Chem. Soc. 112*, 2824 – 2826.

7. Gruff, E. S. and Koch, S. A. (1990) Trigonal-planar $[M(SR)_3]^{1-}$ complexes of cadmium and mercury. Structural similarities between mercury-cysteine and cadmium-cysteine coordination centers. *J. Am. Chem. Soc. 112*, 1245 – 1247.

8. Santos, R. A., Gruff, E. S., Koch, S. A. and Harbison, G. S. (1991) Solid-state mercury-199 and cadmium-113 NMR studies of mercury- and cadmium-thiolate complexes. Spectroscopic models for $[Hg(SCys)_n]$ centers in the bacterial mercury resistance proteins. *J. Am. Chem. Soc. 113*, 469 – 475.

9. Deivaraj, T. C., Dean, P. A. W., and Vittal, J. J. (2000) Synthesis, Structure, and Multi-NMR Studies of $(Me_4N)[A\{M(SC\{O\}Ph)_3\}_2]$ (A = Na, M = Hg; A = K, M = Cd or Hg). *Inorg. Chem. 39*, 3071 – 3074.

10. Baba, K., Okamura, T., Yamamoto, H., Yamamoto, T., and Ueyama, N. (2008) Zinc, Cadmium, and Mercury 1,2-Benzenedithiolates with Intramolecular NH···S Hydrogen Bonds. *Inorg. Chem. 47*, 2837 – 2848.

11. Alsina, T., Clegg, W., Fraser, K. A. and Sola, J. (1992) [Homoleptic cyclohexanethiolato complexes of mercury(II). J. *Chem. Soc. Dalton Trans. 8*, 1393 – 1399.

12. Bramlett, J. M., Im, H.-J., Yu, X.-H., Chen, T., Cai, H., Roecker, L. E., Barnes, C. E., Dai, S., and Xue, Z.-L (2004) Reactions of thioether carboxylic acids with mercury(II). Formation and X-ray crystal structure of mercury(II) mercaptoacetate. *Inorg. Chim. Acta 357*, 243 – 249.

13. Hoffmann, G. G., Steinfatt, I., Brockner, W,. Kaiser, V., and Naturforsch, Z. (1999) Bis(n-pentanethiolato)mercury(II), $Hg(SC_5H_{11})_2$. Preparation, characterization, crystal and molecular structure; reactivity towards organic thiols. *B: Chem.Sci. 54*, 887 – 894.

14. Chieh, C. (1978) Crystal structure of mercury(II) bromide dithiocarbamate, $[HgBr_2(S_2CNEt_2)Hg(S_2CNEt_2)]_n$, an inorganic polymer. *Can. J. Chem. 56*, 564 – 566.

15. Alsaadi, B. M., and Sandstrom, M. (1982) Crystal and molecular structure of bis(2-mercaptobenzoato-S)mercury(II) monodioxane. *Acta Chem. Scand. A 36*, 509 – 512.

16. Melnick, J. G., Yurkerwich, K., and Parkin, G. (2009) Synthesis, Structure, and Reactivity of Two-Coordinate Mercury Alkyl Compounds with Sulfur Ligands: Relevance to Mercury Detoxification. *Inorg. Chem. 48*, 6763 – 6772.